Available online at www.sciencedirect.com
ScienceDirect
Journal of Molecular Catalysis A: Chemical 281 (2008) 200–206
JOURNAL OF MOLECULAR CATALYSIS A: CHEMICAL
www.elsevier.com/locate/molcata

Synthesis of mixed ZrO_2–TiO_2 oxides by sol–gel: Microstructural characterization and infrared spectroscopy studies of NO_x

R. Pérez-Hernández [a,*], D. Mendoza-Anaya [a], M.E. Fernández [a], A. Gómez-Cortés [b]

[a] *Instituto Nacional de Investigaciones Nucleares, Carr. México-Toluca S/N La Marquesa, Ocoyoacac, Edo. de México C.P. 52750, Mexico*
[b] *Instituto de Física-UNAM, Apdo. Postal 20-364, México 01000 D.F., Mexico*

Available online 21 November 2007

Abstract

Single ZrO_2, TiO_2 and mixed ZrO_2–TiO_2 oxides with various Zr:Ti ratio (90:10, 50:50 and 10:90) were prepared by the sol–gel method. The samples were characterized by DSC, nitrogen adsorption, SEM, XRD, molecular simulation and DRIFT. According to the ZrO_2/TiO_2 ratio, the experimental results reveal that the TiO_2 loading into ZrO_2 had effects on shifts of exothermic peaks towards higher temperature, attributed to transition from amorphous to crystalline phase except in the ZT50 xerogel. The optimum concentration of titania into mixed ZrO_2–TiO_2 oxides to obtain high surface area (∼230 m^2/g) and highly acidic surface was in the equimolar composition. An amorphous XRD pattern was observed in the ZT50 sample, this behaviour was related to the mixed Zr–O–Ti bond formed, which caused an atomic disorder in the structure of the sample and this result was confirmed by molecular simulation. All the oxides were constituted by microspheroid particles regardless of the Zr/Ti molar ratio and crystalline phase. Different kinds of surface nitrates (NO_x, $x = 2, 3$) species were observed on the mixed ZrO_2–TiO_2 samples; these species are formed on Lewis sites and the amount of these species on the surface oxide is intimately related to the support acidity, which in turn depends on the specific area of the samples, as well as, on the Zr/Ti ratio and the Zr–O–Ti bond population. Bridged and bidentate NO_3^- species are adsorbed on the Zr-rich samples.

Keywords: ZrO_2–TiO_2 mixed oxides; Acidic properties; Mixed Zr–O–Ti bond; Structural and morphological characterization; NO_x adsorption

1. Introduction

Sol–gel chemistry has been applied to many mixed oxide systems for preparation of glasses, coatings, and other ceramic materials. This technique provides the ability to control molecular-scale mixing and the ability to form the M_1–O–M_2 bonds (where M_1 and M_2 denote two different cations). Combination of dissimilar oxides also presents the potential for creating surface acid sites that are not present in either of the pure components. The reasons for these mixed oxides are they play a central role in chemical and petrochemical processing as catalysts and support for catalytic active species. A major component oxide can be stabilized against degradation of its textural properties upon heat treatment by introduction of even smaller amount of a minor component, thereby allowing the material to be used at more severe processing conditions. For example, several authors have reported that the addition of less than 10 mol% of silica to titania results in significant increments in both surface area and pore volume and delays the crystallization of titania to higher temperatures [1–5]. These effects have been related to the silica's ability to impede titania's normal sintering processes through formation of Ti–O–Si "hetero-linkages" [6]. Solid acid catalysts have the additional advantage that the nature of the active sites are known and may be defined by the presence of surface protons generating Bronsted acidity or co-ordinately unsaturated cationic centers, i.e. Lewis acid sites [7]. Therefore, much attention has been focussed on the development of mixed oxides catalysts [8]. ZrO_2–TiO_2 system are strong solid acids showing catalytic activity in different acid catalyzed reactions, such as isomerization and cracking alkanes, hydration and polymerisation of alkenes [9,10]. Other important issues for these systems are related with fast and direct environmental impact, where catalysts like hazardous liquid acid and base catalysts, such as HF, H_2SO_4, HCl, $Ca(OH)_2$, etc. used by several oil refineries

* Corresponding author. Tel.: +52 55 53 29 72 39; fax: +52 55 53 29 72 40.
E-mail address: pehr@nuclear.inin.mx (R. Pérez-Hernández).

1381-1169/$ – see front matter © 2007 Elsevier B.V. All rights reserved.
doi:10.1016/j.molcata.2007.11.008

and chemical industries can be replaced by mixed oxides. The breakthrough came with the development of solid acid and base catalysts [11] is gradually gaining importance in the catalytic field and it is also possible to develop more. On the other hand, it has been shown that ZrO_2–TiO_2 system can be satisfactorily used as catalytic support for the selective catalytic reduction (SCR) reaction of the NO with hydrocarbons, because, the mixed oxide displays unusual acid properties and very high-thermal resistance respecting to its individual ZrO_2 and TiO_2 components [12–16] and selective catalysts by the incorporation of a transition metal [15,16].

The aim of the current work was to investigate the additive effect of TiO_2 to ZrO_2 on the structure, morphology and textural properties studied by TGA/DSC, XRD, SEM, N_2 adsorption, DRIFT and molecular simulation, the last was used to infer the formation of Zr–O–Ti bond in the mixed ZrO_2–TiO_2 oxide.

2. Experimental

2.1. Single oxides

ZrO_2 and TiO_2 were prepared by sol–gel method from zirconium(IV) propoxide (Fluka) or titanium(IV) propoxide (Fluka) as a precursor in *n*-propanol (Aldrich) solution and basic catalyst (NH_4OH) (Fluka) with constant stirring. The mixed ZrO_2–TiO_2 oxides (10, 50, 90 mol% of TiO_2 in samples) were prepared as follows: mixtures of the alkoxide precursors were used as starting material at appropriate composition in *n*-propanol and NH_4OH with constant stirring. After that, the solution was processed at reflux temperature and the water was added drop wise to the solution at this temperature. The reflux was continued for 1 h and the resultant mixture was cooled at room temperature and aged for 24 h. The residual liquid was removed by decanting and washed two times with deionised water.

The molar ratio used for the synthesis was propoxide/alcohol/H_2O/NH_4OH = 1:4:4:0.33. The xerogel was obtained after heating in an oven at 100 °C for 24 h in static air using a temperature ramp of 5 °C/min. Then the xerogels were calcined at 100 °C for 1 h next the temperature was raised to 500 °C and kept for 5 h. The labelling of different oxides will be referred as ZrO_2, TiO_2 and ZT*n*, where Z = ZrO_2, T = TiO_2, *n* = 10, 50, 90 mol% of TiO_2 in mixed oxide, respectively.

3. Characterization

DSC of xerogel was performed in a DSC-10 from TA-Instruments under N_2 atmosphere in the range of 20–600 °C at a heating rate of 10 °C/min. Total surface area was calculated by the BET method from N_2 adsorption by the single-point method using a 30% N_2/He gas mixture, recorded at the temperature of liquid nitrogen in a RIG-100 multitask characterization unit from ISRI. Samples were first degassed at 150 °C for 1.5 h to eliminate moisture. The morphology and chemical composition analysis of the samples were performed in a Philips XL-30 SEM instrument, fitted with energy dispersive X-ray spectrometer (EDS). Before the analysis, samples were fixed on the specimen holder with an aluminium tape and mounted on an aluminium specimen holder, obtaining the images with the backscattering electron signal with acceleration voltage of 20 kV. Powder X-ray diffraction patterns were recorded with a Siemens D-5000 diffractometer using Cu Kα (λ = 0.15406 nm) all samples were scanned in the range between 2θ = 15–70°. Diffuse reflectance infrared fourier transformed spectra (DRIFT) were collected on a Nicolet-Nexus 670 FT-IR, E.S.P. FT-IR spectrophotometer working at a resolution of 4 cm^{-1}, equipped with a high temperature environmentally controlled cell (Spectra Tech). About 0.030 g of the powdered oxide was packed in a sample holder and pretreated *in situ* in the DRIFT cell under a H_2 flow, then the temperature was increased at a rate of 10 °C/min up to 500 °C and kept for 1 h, after that the oxide was cleaned for 30 min with He flow. The sample was subsequently cooled to 100 °C in He prior to exposure to the mixture of NO (2500 ppm) and 2% O_2 gas mixture, after 15 min of passing the mixture, the sample was purged with He and cooled at room temperature (RT). The DRIFT spectra were collected after 15 min at RT collecting 256 scans.

4. Simulation method

The model for ZrO_2 and TiO_2 interface (ZT50) were built in the (1 0 1) directions according to the crystalline data of the tetragonal unit cell of the ZrO_2 (*a* = 3.570 Å, *c* = 5.16 Å) and TiO_2 (*a* = 3.78 Å, *c* = 9.51 Å). The interface was grown in [0 1 0] direction with 3 Å of thickness for "*a*" and 10 Å for "*b*" and "*c*" parameters in the cell respectively for both oxides, in order to determine the electronic charge density and stability of Zr–O–Ti bond. Quantum mechanics calculations were made through the Cerius^2 program. The calculus is based on density functional theory (DFT) which uses the local density approximation (LDA) and generalized gradient approximation (GGA) to achieve geometrical optimization and determine the charge density [17]. The simulated XRD pattern of the model structure after the geometry optimization was acquired by Bragg Law Theory with Cerius^2 program [18]. The diffraction pattern was obtained by simulating a Siemens D-5000 diffractometer using an X-ray source of copper, with a λ = 0.1540 nm and the scanned 2θ° was from 15° to 80°. The calculations were made in a supercomputer Origin 2000 of Silicon Graphics with 8 R10000 processors.

5. Results and discussion

5.1. Thermal analysis (TGA/DSC)

The TGA curves of the xerogels, (not presented) showed a similar behaviour in their weight loss. In general, the weight loss of the samples was about 10% and it was attributed to the elimination of the physically adsorbed water, physically and chemically adsorbed alcohol and residual organic material coming from the synthesis. Fig. 1 shows DSC profile corresponding to the xerogels, all of them have an endothermic peak from 30 to 250 °C and, it corresponds to the removal of the physically adsorbed water and alcohol [15,19,20]. The exothermic peak at 424 °C observed on the zirconia xerogel, was assigned to

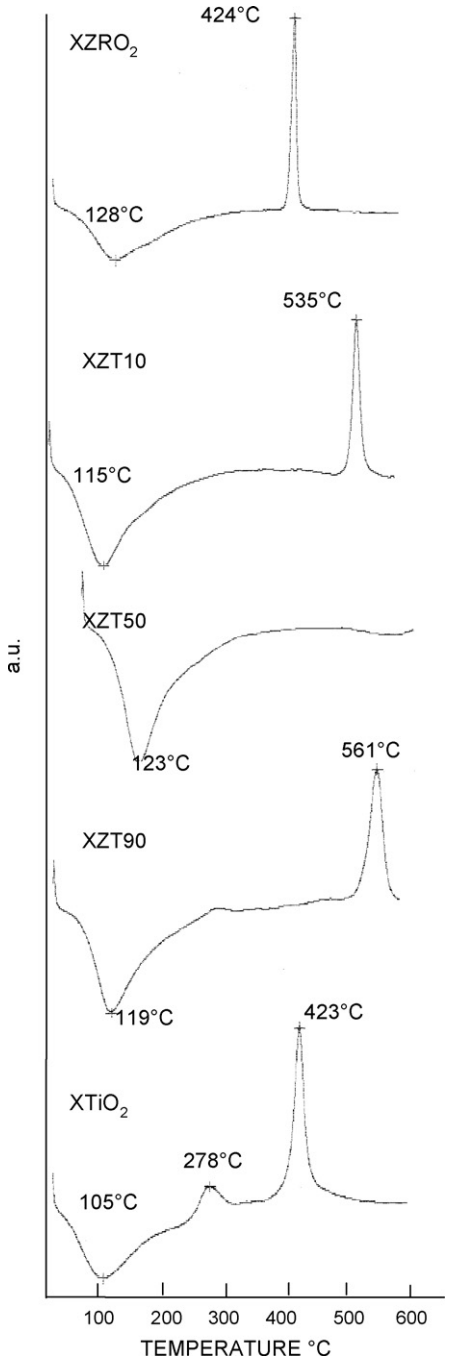

Fig. 1. Differential scanning calorimetric curves of ZrO_2–TiO_2 xerogels.

a change of phase from an amorphous material to crystalline tetragonal zirconia [15,21,22]. For the TiO_2 xerogel, this peak was observed at 423 °C and corresponds to the crystallization of the anatase phase [15,19,20], another peak was observed close to 300 °C and it could be attributed to the decomposition and burning of organic groups [15,19,22]. The increase in the titania or zirconia content on the mixed ZrO_2–TiO_2 xerogels, cause a shift on the exothermic peaks towards higher temperature compared to the single xerogels. These peaks are attributed to the crystallization of the amorphous material. On the ZT10 and ZT90 xerogels the crystallization of the tetragonal (ZrO_2) and anatase

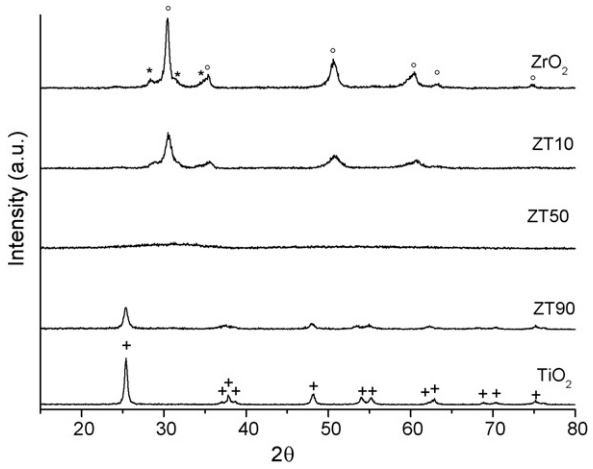

Fig. 2. XRD patterns of ZrO_2–TiO_2 oxides calcined at 500 °C. *: monoclinic, °: tetragonal phases from zirconia and +: anatase-TiO_2.

(TiO_2) phases were observed at 535 and 561 °C, respectively. However, the ZT50 sample did not show an exothermic peak related to the phase transition, from an amorphous phase to a crystalline one up to 600 °C. These results demonstrated that the presence of the titania on zirconia in the mixed oxide delays the formation of $ZrTiO_4$ compound. An exothermic peak was reported on ZrO_2–TiO_2 samples at 600–700 °C and it was associated with the crystallization of amorphous material [21,23]. On the other hand, in the Zr-rich samples an exothermic peak related with the burning of organic material was not observed, this could be associated to the particular set of preparation conditions used in this work.

5.2. Crystalline phases (XRD)

Fig. 2 shows the XRD patterns of the TiO_2 and ZrO_2 samples and mixed ZrO_2–TiO_2 oxides. The XRD pattern of the pure ZrO_2 sample shows a mixture of two crystalline structures; in this case a large predominance of the tetragonal phase and a small amount of monoclinic phase of zirconia were present. While in XRD pattern of the bare TiO_2, the crystalline structure was consistent with the anatase phase. The addition of TiO_2 to ZrO_2 diminishes the intensity of the diffraction peaks and it was interpreted as a lose of the crystallinity in the mixed oxides. ZrO_2-rich oxide showed the same crystalline phases identified in the bare ZrO_2. Meanwhile, for the TiO_2-rich sample, the anatase was the unique phase observed. The XRD pattern of the mixed ZT50 oxide was consistent with an amorphous material, even when the solid was calcined until 600 °C during 8 h. This result is in agreement with DSC results for this oxide, which did not show an exothermic peak related with the phase transformation from amorphous to crystalline material. An amorphous material was reported [15,23] in the ZrO_2–TiO_2 samples independently of the route of the synthesis in the mixed oxides. The amorphous ZT50 sample could be favoured by decreasing the particle size of the material [15]. However, crystallization of amorphous ZT50 oxide to $ZrTiO_4$ phase is reported above 600 °C [21,23–25] regardless the method of synthesis.

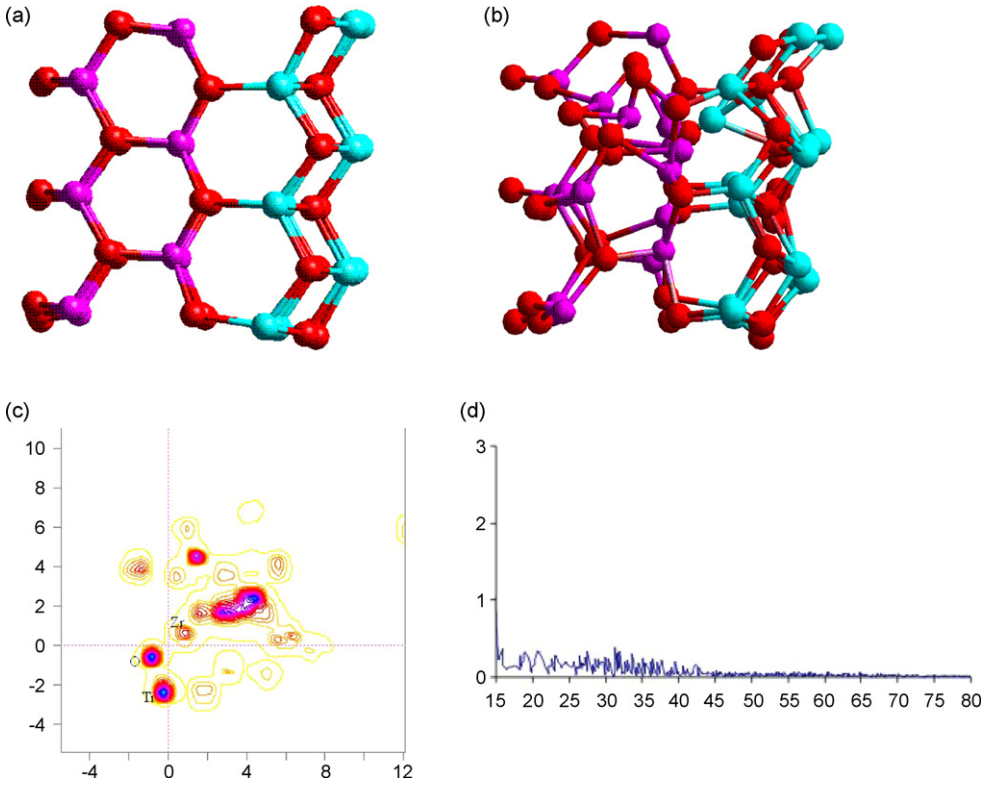

Fig. 3. (a) Surface of initial model of mixed ZrO_2–TiO_2 bond; (b) surface model after de relaxation process; (c) pattern slice of electronic charge density from (b); (d) XRD pattern from (b).

5.3. Analysis of the Zr–O–Ti bond by quantum mechanics

Fig. 3(a–d) shows the molecular simulation results of the mixed ZT50 oxide. Fig. 3a shows the theoretical model of the interface with the same Zr–O and Ti–O bonds before the relaxation process used to determine if the Zr–O–Ti bond is stable on the mixed oxides and how this bond affects the crystalline structure of the samples. After the relaxation process the original symmetry of the model was distorted as is shown in Fig. 3b. Fig. 3c shows the map of the electron charge density (ECD) of pattern slice from the model after relaxation process. From this map it can be seen that the ECD is distributed around the mixed bond, which confirms the existence of the mixed Zr–O–Ti link. However, the map of ECD showed clearly that the charge density is concentrated on the Ti–O bond, causing a deficiency of charge in the Zr^{+4} cation; which could probably act as an adsorption centre for the catalytic reaction. Thus the generation of mixed Zr–O–Ti bond, leads to electron transfer from Zr–O bond to Ti–O link and causes the new distribution of charge on the mixed link. On the other hand, the XRD pattern of the ZT50 model obtained after the relaxation process was consistent with an amorphous material (Fig. 3d). Therefore, the atomic disorder of the mixed Zr–O–Ti bond in the lattice structure is caused by the incorporation of the Zr^{+4} or Ti^{+4} cations into the host matrix (ZrO_2 or TiO_2) producing an amorphous material. This result confirms that the mixed Zr–O–Ti bonds are responsible for the lose of the crystallinity and corroborate our experimental XRD result for the ZT50 oxide. Xu et al. [23] studied EXAFS and XANES of the $ZrTiO_4$ samples synthesized by different routes. They suggested the presence of the mixed Zr–O–Ti links in the dry and calcined samples up to 600 °C in which the solids were amorphous.

5.4. Textural properties (BET, SEM)

The surface area of the two pure oxides is 10 and 29 m^2/g for ZrO_2 and TiO_2, respectively. In the mixed oxides the surface area was increased proportionally to the titania loading to zirconia until an equimolar composition was reached in comparison with the single oxides. For ZT10 and ZT90 oxides the surface area is 71 and 80 m^2/g, respectively. For the sample with equimolar composition the surface area reached a maximum up to 232 m^2/g. It is clear that the ZrO_2–TiO_2 samples with higher surface area also show the high-temperature transition phase (Fig. 1) and low crystallinity. Fig. 4 shows the SEM image corresponding to ZrO_2 and TiO_2 calcined at 500 °C. It can be seen that both samples are conformed by particles with spherical tendency and, a zirconia particle size of 0.3 μm, while for TiO_2 it was 0.9 μm. A spherical tendency was also observed for mixed oxides, but the particle size found was between 0.3–0.9 μm.

5.5. NO and O_2 co-adsorption over ZrO_2–TiO_2

In situ DRIFT spectra of the single and mixed ZrO_2–TiO_2 oxides exposed to a $NO + O_2$ gas mixture were recorded at room temperature with the aim to evaluate the influence of the surface acidity on the type and amount of different surface species.

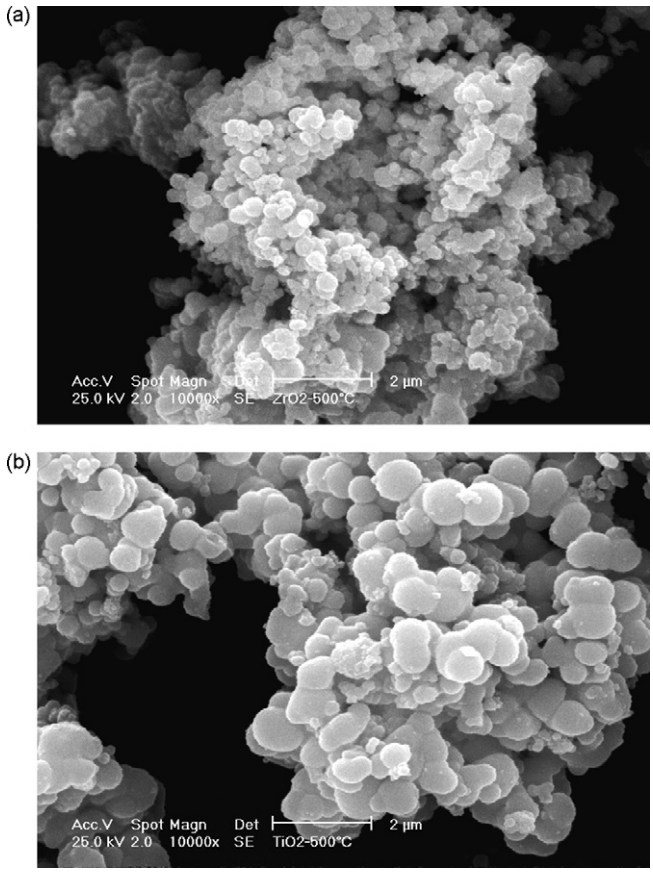

Fig. 4. SEM micrographs of ZrO_2–TiO_2 oxide calcined at 500 °C. (a) ZrO_2 and (b) TiO_2.

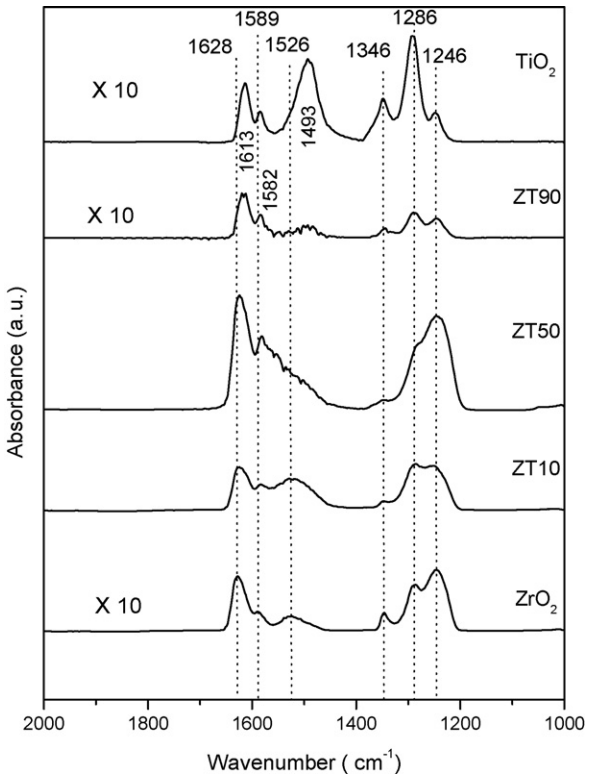

Fig. 5. DRIFT spectra of NO and O_2 co-adsorption at room temperature on mixed ZrO_2–TiO_2 oxides.

Several authors have reported that the role of the acid sites in the samples is to promote the NO oxidation step [26–29] during SCR reaction of NO with hydrocarbons. Fig. 5 shows an infrared spectra in the 2000–1000 cm^{-1} region of the ZrO_2–TiO_2 oxides. In general, the absorption bands in the 1350–1200 cm^{-1} range are the same independently of the ZrO_2/TiO_2 ratio but the intensity is influenced by the percentage of each one of the oxides in the mixed samples. The bands at 1286 and 1246 cm^{-1} increase their intensity when titania is loaded to the zirconia until the composition reached ZT50; however, the later band is larger than the former. For the ZT90 oxide these bands are very weak and again they increase for the single TiO_2. It is clear that the band at 1246 cm^{-1} in the titania is weaker than in zirconia.

The bands in the 1650–1400 cm^{-1} range are shifted to lower wavenumbers as a function of titania loading into zirconia. The positions of the peaks at 1628, 1589 and 1526 cm^{-1} observed on the ZrO_2-rich samples are shifted to 1613, 1582 and 1493 cm^{-1}, respectively in the TiO_2-rich samples. Besides, it is evident that as TiO_2 is loaded to ZrO_2 in the mixed oxides, the bands at 1628, 1589 and 1526 cm^{-1} increase their intensity until ZT50 sample, after this, the intensity diminishes again. The specie adsorbed at 1628 cm^{-1} on ZrO_2 is practically the same until the composition is reached ZT50. However, the band at 1589 cm^{-1} shifts to 1582 cm^{-1} from ZT10 until TiO_2 samples. Although the band at 1526 cm^{-1} observed on the ZrO_2 and ZT10 samples becomes a broad band in the ZT50 sample, for the TiO_2-rich samples this band shift to 1493 cm^{-1}. Therefore, we can affirm that the species adsorbed at 1628 and 1526 cm^{-1} prefer the zirconia entities, while the species at 1582 cm^{-1} are adsorbed on titania entities on the ZrO_2–TiO_2 oxides.

The assignments of absorption bands described above are consistent with those reported previously on ZrO_2 or TiO_2 and are classified as nitrite/nitrate species [14,30–34]. Free nitrite ion (NO_2^-) has been reported at 1250 ($\nu_{as}(NO_2)$) cm^{-1} [35]. Hadjiivanov [36], Kantcheva [32] and Watson et al. [37] attributed the band at 1240 cm^{-1} to bidentate nitrate (NO_3^-) species formed on ZrO_2, Mn/TiO_2 and titanium oxide surfaces, respectively. Whereas, the band near 1286 cm^{-1} has been attributed to the monodentate nitrates (NO_3^-) on TiO_2 [32], nitro species on ZrO_2 [36] and $\nu_{as}(NO_2)$ on $CuSO_4$/ZrO_2 [33]. For the Pt/ZrO_2–TiO_2 catalysts this band was attributed to NO stretching modes of bidentate nitrate [16]. The bands at 1320–1340 cm^{-1} were assigned to nitro species in the form of M–NO_2 [35,38] and chelated nitro ($\nu_s(NO_2)$) [33]. In this work the bands at 1286 and 1246 cm^{-1} are assigned to nitro and nitrate species adsorbed on Zr^{+4} or Ti^{+4} cations from the bare oxides respectively, these bands increase their intensity as TiO_2 is loaded to ZrO_2 until an equimolar composition, as a result of the generation of the mixed Zr–O–Ti bonds which promote the absorption centres for those species. The nitrate species observed at 1246 cm^{-1} is preferably adsorbed on Zr^{+4} cation; because on ZT90 and TiO_2 oxides this NO^-_3 is not stable (their intensity is very low).

The absorption bands in the 1650–1400 cm^{-1} range are typical of different kinds of surface nitrate species [30,38,39].

Table 1
Possible structures of surface NO_3^- and NO_2^- species on ZrO_2–TiO_2 oxides

Sample	Frequency (cm^{-1})	Possible assignment
ZrO_2	1628	Zr^{+4}–NO_3^- (s-bridged)
	1589	Zr^{+4}–NO_3^- (s-bidentate)
	1526	Zr^{+4}–NO_2 (s-bridge-nitro)
	1346	Zr^{+4}–NO_2 (w-nitro)
	1286	Zr^{+4}–NO_2 (s-nitro)
	1246	Zr^{+4}–NO_3^- (s-bidentate)
ZT10	1628	Zr^{+4}–NO_3^- (s-bridged)
	1582	Ti^{+4}–NO_3^- (s-bidentate)
	1526	Zr^{+4}–NO_2 (s-bridge-nitro)
	1346	Zr^{+4} and Ti^{+4}–NO_2 (w-nitro)
	1286	Zr^{+4}–NO_2 (s-nitro) and Ti^{+4}–NO_3^- (w-bidentate)
	1246	Zr^{+4}–NO_3^- (s-bidentate) and Ti^{+4}–NO_3^- (w-bidentate)
ZT50	1626	Zr^{+4}–NO_3^- (s-bridged)
	1582	Ti^{+4}–NO_3^- (s-bidentate)
	1526	Zr^{+4}–NO_2 (s-bridge)
	1346	Zr^{+4} or Ti^{+4}–NO_2 (w-nitro)
	1286	Zr^{+4}–NO_2 (s-nitro) and NO_3^- (bidentate)
	1246	Zr^{+4}–NO_3^- (s-bidentate) and Ti^{+4}–NO_3^- (w-bidentate)
ZT90	1613	Ti^{+4}–NO_3^- (w-bidentate) or Ti^{+4}–NO_3^- (w-bridged)
	1582	Ti^{+4}–NO_3^- (w-bidentate)
	1493	Ti^{+4}–NO_2 (w-bridge nitro-nitro)
	1346	Zr^{+4} and Ti^{+4}–NO_2 (w-nitro)
	1286	Zr^{+4}–NO_2 (w-nitro) and Ti^{+4}-NO_3^- (w-monodentate)
	1246	Zr^{+4}–NO_3^- (w-bidentate) and Ti^{+4}–NO_3^- (w-bidentate)
TiO_2	1613	Ti^{+4}–NO_3^- (bidentate) or Ti^{+4}–NO_3^- (bridged)
	1582	Ti^{+4}–NO_3^- (bidentate)
	1493	Ti^{+4}–NO_2 (bridge nitro-nitro)
	1346	Ti^{+4}–NO_2 (w-nitro)
	1286	Ti^{+4}–NO_3^- (s-monodentate)
	1246	Ti^{+4}–NO_3^- (w-bidentate)

S = strong, w = weak.

The band at 1640–1630 (ν(N=O)) cm^{-1} has been reported as bridged NO_3^-, bidentate NO_3^- at 1615–1550 (ν(N=O)) cm^{-1} and bridged nitro (NO_2^-) at 1545–1530 ($\nu_{as}(NO_2^-)$) cm^{-1} [14,33,34,40] on catalysts using ZrO_2 as a support. Delahay et al. [40] assigned the band at 1590 cm^{-1} to the nitrate species adsorbed on ZrO_2. Kantcheva [32] has reported formation of bidentate nitrates (NO_3^-) at 1615 and 1580 cm^{-1}, while, adsorbed NO_2 was tentatively assigned at 1610 cm^{-1} on TiO_2 and bridged nitro-nitrite (NO_2^-) at 1487 cm^{-1} on MnO_x/TiO_2. Watson and Ozkan [37] assigned the band at 1618 cm^{-1} to the bridged nitrate and the band at 1580 cm^{-1} to the bidentate nitrate specie formed on reduced TiO_2. When NO was adsorbed on TiO_2, bands at 1616 and 1580 cm^{-1} were observed and assigned to nitrate species [41]. Chien et al. [42] reported the formation of bidentate NO_3^- species at 1607 and 1584 cm^{-1} adsorbed on TiO_2 surface. Nitrate species can be formed by disproportionation of NO_2 (produced by oxidation of NO with O_2) [39,43,44] at the Lewis acid–base pairs [30]. Tanabe et al. [45] predict the Lewis acid for the zirconia-rich mixed oxide; while in the titania-rich mixed oxide predict the Brönsted acid. Lahousse et al. [46] reported for the mixed ZrO_2(23%)–TiO_2(77%) oxide the existence of the Brönsted acidity. These results could explain the phenomena observed in the spectra of the ZT90 oxide which clearly indicates that the oxidation of NO by O_2 is irrelevant, for that on this sample the Lewis acidity is extremely low. Yung et al. [47] characterized by DRIFT technique at the Co/ZrO_2 catalyst and found that the bidentate and bridging nitrates still remain up to 350 °C. Ito et al. [48] observed by DRIFT that the nitrate (NO_3) specie is strongly adsorbed into ZrO_2–TiO_2 samples, they concluded that these materials could be used as NO_x adsorbent at the range of composition of $(n)TiO_2$–$(1-n)ZrO_2$ between $n = 0.25$–0.50. Takahashi et al. [49] reported high NO_x storage at temperatures >500 °C < 600 °C on the ZrO_2–TiO_2 samples with 70% and 80% of ZrO_2.

The above IR bands observed on the bare ZrO_2 and TiO_2 and ZrO_2–TiO_2 samples are assigned to inorganic NO_x^- ($x = 2$, 3) species formed on Lewis acid sites. The amount of these species on the surface oxides is intimately related to support acidity, which in turn depends on the specific area of the support [14], as well as on the enlargement of the mixed Zr–O–Ti bond population and the Zr/Ti ratio in the range of ZT(100–n) between $n = 90$–10. It could be possible that when the electrons of the oxygen of the Zr–O bond from Zr–O–Ti link is strongly attracted by Ti^{+4} ion, it causes a delocalization of ECD in the Zr^{+4} ion, (Fig. 3c), consequently NO_x^- bond is formed on Zr^{+4} ion. Because of this the selective adsorption of bidentate or bridged NO_3^- and nitro species reached a maximum between 1628 and 1613, 1286 and 1246 cm^{-1} bands for ZrO_2, ZT10 and ZT50 samples. Table 1, shows the possible NO_x^- ($x = 2$, 3) species adsorbed on the mixed ZrO_2–TiO_2 oxides.

6. Conclusions

ZrO_2–TiO_2 mixed oxides were synthesized by sol–gel method and characterized by DSC, XRD, SEM, N_2 adsorption, molecular simulation and DRIFT. DSC showed a shift of the exothermic peak towards high temperature, attributed to transition from the amorphous to crystalline phase except on the ZT50 xerogel. Surface area of the oxides was modified depending of the molar ratio of the ZrO_2/TiO_2. Single and mixed oxides showed morphologies constituted by microspheroids aggregates independently of the ZrO_2/TiO_2 molar ratio and crystalline structure, indicating a homogeneous kinetics of nucleation of the microspheroids during the synthesis. XRD results showed that the crystalline phases of the mixed oxides diminish progressively as the titania is loaded to the zirconia until the equimolar composition. On Zr-rich oxides the tetragonal and monoclinic phases were observed, while anatasa phase was identified on titania-rich oxides. In the mixed oxide with equimolar composition an amorphous material was obtained. In any case, we did not observe a segregation of phases on the mixed oxides indicating a high solubility of TiO_2 or ZrO_2 in the host oxide.

Zr–O–Ti mixed bond promotes the lose of crystalline phase on the ZrO_2–TiO_2 mixed oxides, which reaches their maximum for the sample with equimolar composition as has been demonstrated by molecular simulation, as well as the delocalization of electrons in Zr^{+4} cation. The modification in the electron charge density of the Zr–O–Ti link can be acting as adsorption centres for NO_x^-. On the ZrO_2–TiO_2 samples different kinds of the surface nitrates are observed and these are formed on the Lewis sites. The amount of these species on the surface oxide is intimately related to the support acidity, which depends on the specific area of the ZrO_2–TiO_2. On the mixed Zr–O–Ti bond population and on Zr/Ti ratio in the range of $(n)ZrO_2$-$(100–n)TiO_2$ when ≤ 90 $n \geq 50$. On ZT10 sample the presence of NO_x^- species is larger than in ZT90 oxide. However, the Zr-rich samples preferred the adsorption of the bridged NO_3^- and nitro species.

Acknowledgements

Thanks to I.Q. Leticia Carapia for technical support and to the projects ININ-CA-711 and CONACyT (México) J-48924 for financial support.

References

[1] J.B. Johnston, S.T. Miller, E.I. Ko, J. Catal. 150 (1994) 311–320.
[2] J.R. Sohn, H.J. Jang, M.Y. Park, E.H. Park, J. Mol. Catal. 93 (1994) 149–167.
[3] Z. Liu, J. Tabora, R.J. Davis, J. Catal. 149 (1994) 117–126.
[4] C. Ingemar-Odenbrand, J.G.M. Brandin, G. Busca, J. Catal. 135 (1992) 505–517.
[5] Ji-jian Cheng, Dong-wei Wang, J. Non-Cryst. Solids 100 (1988) 288–291.
[6] K. Karmakar, D. Ganculi, Indian J. Technol. 25 (1987) 282.
[7] A. Corma, Chem. Rev. 95 (1995) 559–614.
[8] H. Tanaka, M. Boulinguiez, M. Vrinat, Catal. Today 29 (1996) 209–213.
[9] K. Tanabe, M. Misono, Y. Ono, H. Hattori, New Solids and Bases, Kodansha–Elsevier, Tokyo, 1989, p. 199.
[10] T. Yamaguchi, Appl. Catal. 61 (1990) 1–25.
[11] K. Arata, Adv. Catal. 37 (1990) 165.
[12] M. Haneda, Y. Kintaichi, M. Inaba, H. Hamada, Bull. Chem. Soc. Jpn. 70 (1997) 499–508.
[13] E.P. Reddy, T.C. Rojas, A. Fernández, Langmuir 16 (2000) 4217–4221.
[14] R. Mariscal, S. Rojas, A. Gómez-Cortés, G. Díaz, R. Pérez, J.L.G. Fierro, Catal. Today 75 (2002) 385–391.
[15] R. Pérez-Hernández, A. Gómez-Cortés, J. Arenas-Alatorre, S. Rojas, R. Mariscal, J.L.G. Fierro, G. Díaz, Catal. Today 107/108 (2005) 149–156.
[16] M. Machida, S. Ikeda, D. Kurogi, T. Kijima, Appl. Catal. B: Environ. 35 (2001) 107–116.
[17] M.E. Fernández, C. Zorrilla-Cangas, R. García-García, J.A. Ascencio, J. Reyes-Gasga, Acta Cryst. B B 59 (2003) 175–181.
[18] Molecular Simulation Inc., 1997, Cerius2. Molecular and Quantum Mechanics and Analytical Instruments, San Diego, California.
[19] J.P. Perdew and Y. Wang, Phys. Rev. B, 45, 13244.
[20] I.A. Montoya, T. Viveros, J.M. Domínguez, L.A. Channels, I. Schifter, Catal. Lett. 15 (1992) 207–217.
[21] Q. Xu, M.A. Anderson, J. Am. Ceram. Soc. 76 (8) (1993) 2093–2097.
[22] A. Knell, P. Barnickeñ, A. Baiker, A. Wokaun, J. Catal. 137 (1992) 306–321.
[23] J. Xu, C. Lind, A.P. Wilkinson, S. Pattanaik, Chem. Mater. 12 (2000) 3347–3355.
[24] M. Daturi, A. Cremona, F. Milella, G. Busca, E. Vogna, J. Eur. Cer. Soc. 18 (1998) 1079–1087.
[25] H. Zou, Y.S. Lin, Appl. Catal. A: Gen. 265 (2004) 35–42.
[26] Y. Ly, J.N. Armor, J. Catal. 145 (1994) 388–399.
[27] J.O. Petunchi, W.K. Hall, Appl. Catal. B 2 (1993) L17–L26.
[28] C.J. Loughran, D.E. Resasco, Appl. Catal. B 7 (1995) 113–126.
[29] E. Kikuchi, K. Yogo, Catal. Today 22 (1994) 73–86.
[30] K.I. Hadjivanov, Catal. Rev. Sci. Eng. 42 (1/2) (2000) 71–144.
[31] Y. Kintaichi, M. Haneda, M. Inaba, H. Hamafa, Catal. Lett. 48 (1997) 121–127.
[32] M. Kantcheva, J. Catal. 204 (2001) 479–494.
[33] M. Kantcheva, Appl. Catal. B 42 (2003) 89–109.
[34] M. Kantcheva, A.S. Vakkasoglu, J. Catal. 223 (2004) 352–363.
[35] K. Nakamoto, Infrared an Raman Spectra of Inorganic and Coordination Compounds, Part B, 5th ed., Wiley, New York, 1997.
[36] K. Hadjiivanov, Catal Lett. 68 (2000) 157–161.
[37] J.M. Watson, U.S. Ozkan, J. Catal. 210 (2002) 295–312.
[38] S.-J. Huang, A.B. Walters, M.A. Vannice, J. Catal. 192 (2000) 29–47.
[39] M. Kantcheva, E.Z. Ciftlikli, J. Phys. Chem. B 106 (2002) 3941.
[40] G. Delahay, B. Coq, E. Ensuque, F. Figuéras, Langmuir 13 (1997) 5588–5592.
[41] K. Hadjiivanov, H. Knözinger, Phys. Chem. 2 (2002) 2803.
[42] S.-H. Chien, M.-C. Kuo, C.-H. Lu, K.-N. Lu, Catal. Today 97 (2004) 121–127.
[43] M.M. Kantcheva, V.P. Bushev, K.I. Hadjiivanov, J. Chem. Soc., Faraday Trans. 88 (1992) 3087–3089.
[44] K. Hadjiivanov, V. Bushev, M. Kantcheva, D. Klissurski, Langmuir 10 (1994) 464–471.
[45] K. Tanabe, T. Sumiyoshi, K. Shibata, T. Kiyoura, J. Kitagawa, Bull. Chem. Soc. Jpn. 47 (5) (1974) 1064–1066.
[46] C. Lahousse, A. Aboulayt, F. Maugé, J. Bachelier, J.C. Lavalley, J. Mol. Catal. 84 (1993) 283–297.
[47] M.M. Yung, E.M. Holmgreen, U.S. Ozkan, J. Catal. 247 (2007) 356–367.
[48] K. Ito, S. Kakino, K. Ikeue, M. Machida, Appl. Catal. B: Environ. 74 (2007) 137–143.
[49] N. Takahashi, A. Suda, I. Hachisuka, M. Sugiura, H. Sobukawa, H. Shinjoh, Appl. Catal. B: Environ. 72 (2007) 187–195.